African Multidisciplinary
Journal of Sciences and Artificial Intelligence

ISSN : 1595-7969

Index: Harvard, Boston, Sydney University, Dimensions, Lens, ResearchGet Scilit, Semantic, Google Scholar, Base etc

https://doi.org/10.58578/AMJSAI.v3i1.9189

Fractional-Order Modeling and Analysis of Nanoparticle Transport in Magnetohydrodynamic Blood Flow through a Stenosed Artery

Isah Abdullahi[1] & Ali Musa[2]
[1]Abubakar Tafawa Balewa University, Bauchi, Nigeria
[2]Yobe State University Damaturu, Nigeria
isahabdullahi7474@gmail.com

Article Info:

Submitted:	Revised:	Accepted:	Published:
Feb 8, 2026	Mar 8, 2026	Mar 20, 2026	Mar 25, 2026

Abstract

This study presents an extended fractional-order mathematical model for blood flow through a stenosed artery under the combined effects of a magnetic field, porous medium, chemical reaction, and nanoparticle diffusion. The study aims to provide a more accurate and physiologically relevant representation of nanoparticle transport in pathological arterial flow conditions. The governing nonlinear equations for momentum and mass transfer were formulated and solved using a semi-analytical approach involving modified Bessel and Mittag–Leffler functions. Model validation through comparison with existing results showed excellent agreement, confirming the reliability of the proposed formulation. The parametric analysis revealed that increasing the chemical reaction parameter and Schmidt number reduced nanoparticle concentration, whereas a higher fractional order enhanced mass transport by weakening memory effects. The study concludes that the fractional-order framework offers an improved description of nanoparticle transport in stenosed arterial blood flow and contributes to the

advancement of mathematical modeling for physiologically realistic hemodynamic analysis.

Keywords: Fractional-Order Modeling; Nanoparticle Transport; Magnetohydrodynamic Blood Flow; Stenosed Artery; Mass Transfer

Introduction

Cardiovascular diseases continue to constitute a major global health burden, with arterial stenosis being one of the most critical pathological conditions affecting normal blood circulation. Stenosis, which arises from the accumulation of atherosclerotic plaques along arterial walls, leads to vessel narrowing and causes significant alterations in blood flow characteristics, including velocity distribution, shear stress, and mass transport behavior. Early experimental investigations by Ahmed and Giddens (1983) provided foundational insight into pulsatile flow through constricted tubes, demonstrating that unsteady pressure gradients and geometric irregularities profoundly influence arterial hemodynamics. Their work established the importance of pulsatility in accurately modeling physiological blood flow in stenosed vessels.

Blood flow in arteries is inherently complex due to its non-Newtonian rheology and its interaction with multiple physical mechanisms such as magnetic fields, heat transfer, and porous arterial structures. Over the years, magnetohydrodynamic (MHD) models have been widely employed to examine the influence of externally applied magnetic fields on blood flow behavior. Adamu et al. (2020) investigated MHD blood flow through stenosed arteries under inclined magnetic fields and showed that magnetic forces can significantly modify velocity profiles and flow resistance. Similarly, Wang et al. (2022) numerically analyzed pulsatile non-Newtonian blood flow in small vessels under magnetic effects and confirmed that magnetic fields play a vital role in controlling both momentum and heat transfer processes. These findings are particularly relevant to biomedical applications such as magnetic drug targeting and cancer therapy.

The incorporation of nanoparticles into blood flow has further intensified research interest due to their growing applications in targeted drug delivery, tumor treatment, and diagnostic procedures. The theoretical basis for nanofluid transport was established by Buongiorno (2006), who identified Brownian motion and thermophoresis as dominant

mechanisms governing nanoparticle migration in convective flows. Building on this framework, several studies have explored nanofluid behavior in biological and biomedical contexts. Ellahi et al. (2019) examined nanoparticle-laden blood flow under chemical reaction effects and demonstrated that reaction rates significantly influence solute concentration and transport efficiency. Likewise, Sheikholeslami (2018) analyzed nanofluid flow under magnetic and porous medium effects, highlighting the strong coupling between Lorentz forces and nanoparticle dispersion.

Despite the extensive use of integer-order differential models in blood flow analysis, such formulations often fail to capture the inherent memory and hereditary characteristics of biological transport processes. To address this limitation, fractional calculus has emerged as a powerful mathematical tool capable of modeling anomalous diffusion and long-range temporal dependence. Kot and Elmabound (2021) applied fractional calculus to pulsatile blood flow through a stenosed artery and demonstrated that fractional-order models provide better agreement with physiological behavior compared to classical models. In a related study, Jamil et al. (2021) employed Caputo–Fabrizio fractional derivatives to investigate magnetic Casson blood flow in an inclined stenosed artery, confirming that fractional derivatives enhance the modeling of viscoelastic and memory-dependent effects in blood flow.

More recent contributions have further reinforced the applicability of fractional modeling in biofluid dynamics. Alhachami et al. (2024) analyzed time-fractional magnetohydrodynamic viscous fluid flow and reported improved accuracy in transient flow predictions. In the context of reaction–diffusion systems, Che et al. (2022) demonstrated that fractional derivatives reveal novel spatiotemporal patterns and provide a more generalized framework for anomalous transport phenomena. Additionally, Han et al. (2022) developed high-precision numerical techniques for fractional-order diffusion models, offering reliable computational tools for simulating complex biological systems.

In light of these developments, there remains a clear need for a comprehensive mathematical framework that simultaneously accounts for pulsatile blood flow, magnetic field effects, nanoparticle transport, chemical reactions, and memory-dependent diffusion in stenosed arteries. The present study addresses this gap by formulating a fractional-order magnetohydrodynamic model for nanoparticle transport in a stenosed arterial segment. By incorporating Caputo fractional-time derivatives, the model captures anomalous diffusion and hereditary effects that are absent in classical formulations. This approach provides a more

physiologically realistic representation of nanoparticle concentration dynamics and offers valuable insights into biomedical applications such as drug delivery and therapeutic intervention in diseased arteries.

Governing Equation

The concentration equation presented under Section 2.0 describes the transport and distribution of nanoparticles or dissolved chemical species within pulsatile blood flow through a stenosed artery by incorporating the combined effects of molecular diffusion, chemical reaction, and convective transport induced by time-dependent blood motion, as formulated in the governing biofluid models of Wang et al. (2022) and Yakubu et al. (2025) The equation accounts for essential physiological factors such as mass diffusivity, solute concentration, and free-stream concentration, and reflects the influence of oscillatory pressure gradients, body acceleration, and thermal effects associated with pulsatile flow conditions as discussed by Shirt et al. (2015) and Ellahi et al. (2019). It is developed as part of a coupled nonlinear system governing momentum, energy, and mass transfer within a porous stenosed arterial segment, and is later extended through the introduction of Caputo fractional-time derivatives to capture memory effects and anomalous diffusion characteristics typical of complex biological transport processes .The model is supplemented with appropriate initial and boundary conditions to ensure physiological relevance, and its solution provides a detailed representation of the spatial and temporal variation of nanoparticle concentration within the arterial domain

$$\frac{\partial \overline{C}}{\partial \hat{t}} = D\left(\frac{\partial^2 \overline{C}}{\partial \overline{r}^2} + \frac{1}{\overline{r}}\frac{\partial \overline{C}}{\partial \overline{r}}\right) - A(\overline{C} - \overline{C}_0) \qquad (1)$$

Pulsatile flow is essential from both physiological and mathematical perspectives for accurately representing blood flow behavior in arteries, particularly when subjected to external vibrations, oscillatory pressures, or thermal influences. As described in (Shirt et al., 2015 & Ellahi et al., 2019), this pulsatile characteristic is modeled using time-periodic functions that account for body acceleration, pressure gradient, and thermal radiation within a vibrational environment, respectively, as follows; D Mass diffusivity, C Solutes concentration and C_0 Free stream concentration

The above equation governed by the corresponding initial and boundary conditions.

$$\left.\begin{array}{llll} \overline{C} = \overline{C}_0; & \forall \bar{r} \in (0.R_0), & at & \bar{t} = 0 \\ ,\dfrac{\partial \overline{C}}{\partial \bar{r}} = 0; & \forall t > 0, & at & \bar{r} = 0 \\ \overline{C} = \overline{C}_0; & \forall \bar{t} > 0 & at & \bar{r} = \overline{R}(\bar{z}) \end{array}\right\} \quad (2)$$

The symbols $\bar{u}_0, \overline{T}_0, \overline{C}_0,$ maintained their usual meaning, and $\overline{R}(\bar{z})$ represent the equation that models the stenosed region, as stated in (Imoro et al.,2024) as follows:

$$\overline{R}(z) = \begin{cases} \left\{ R_0 - \dfrac{\lambda}{2}\left(1 + \cos(\dfrac{4\pi\bar{z}}{l_0})\right), -\dfrac{l_0}{4} \le \bar{z} \le \dfrac{l_0}{4} \right. \\ R_0, \quad otherwise \end{cases} \quad (3)$$

The symbols l_0 and λ represent the length of the artery and the maximum height of the stenosis, respectively.

These governing equations are supplemented by appropriate initial and boundary conditions reflecting physiological constraints, such as no-slip velocity at the artery wall, specified wall temperature and concentration, and symmetry conditions along the artery centerline.

Solution technique

By employing the following parameters, the equations (1)-(3) can be rendered dimensionless;

$$r = \frac{\bar{r}}{R_0}, z = \frac{\bar{z}}{R_0}, t = \frac{u_0 \bar{t}}{R_0}, R(z) = \frac{\overline{R}(\bar{z})}{R_0}, Q = \frac{\overline{C} - C_0}{C_0 - C_\infty} \quad (4)$$

By applying equation. (4) into eqns. (1-3) and dropping the bars, we have:

$$S_c R_e \frac{\partial Q}{\partial t} = \frac{\partial^2 Q}{\partial r^2} + \frac{1}{r}\frac{\partial Q}{\partial r} - C_r Sc R_e^2 Q \quad (5)$$

$$\left.\begin{array}{llll} Q = Q_0; & \forall r \in (0,1), & at & t = 0 \\ \dfrac{\partial Q}{\partial r} = 0; & \forall t > 0, & at & r = 0 \\ ,Q = Q_0; & \forall t > 0, & at & r = R(z) \end{array}\right\} \quad (6)$$

$$R(z) = \begin{cases} 1 - \dfrac{\lambda}{2R_0}\left(1 + \cos\left(\dfrac{4\pi z R_0}{l_0}\right)\right), -\dfrac{l_0}{4R_0} < z < \dfrac{l_0}{4R_0} \\ 1, \quad otherwise \end{cases} \quad (7)$$

Where

$$Cr = \frac{k_0 \nu}{u_{z0}^2}, Sc = \frac{\nu}{D_m}, \mathrm{Re} = \frac{R_0 u_{z0}}{\nu}$$

are defined as Chemical reaction parameter, Schmidt number and Reynolds number, respectively.

Fractional-Time Derivatives of Modeled Equations

Fractional-order models provide improved precision in representing spatial diffusion and memory effects, making them particularly well-suited for complex biological systems. Advanced numerical techniques for space-fractional models, such as those proposed by Han et al., (2022), have demonstrated high effectiveness in accurately describing diffusion processes, enhancing the stability of fractional differential equations, and offering reliable tools for simulating intricate biological phenomena. The incorporation of Riesz fractional derivatives in reaction–diffusion models, as shown by Che et al., (2022) uncovers novel spatiotemporal behaviors, enhances the accuracy of anomalous transport analysis, and delivers a more generalized framework for biofluid dynamics. Furthermore, the application of fractional calculus in modeling non-Newtonian blood flow is supported by works such as Jamil et al., (2021) who utilized Caputo–Fabrizio fractional derivatives to study magnetic Casson blood flow in inclined stenosed arteries. Likewise, Alhachami et al., (2023) examined time-fractional magnetohydrodynamic flow over a plate, further confirming the effectiveness of fractional derivatives in blood flow analysis. Collectively, these studies highlight the relevance of fractional-time derivatives for capturing the complex dynamics of biological fluids. Accordingly, by introducing the Caputo fractional derivative into the transient terms of Equations (5), we obtain;

$$Sc\,R_e\left(s^{\alpha}\overline{Q}(r,s)-\sum_{m=0}^{n-1}s^{\alpha-1-m}\overline{Q}(r,0)\right)=\left[\frac{\partial^2\overline{Q}(r,s)}{\partial\bar{r}^2}+\frac{1}{\bar{r}}\frac{\partial\overline{Q}(r,s)}{\partial\bar{r}}\right]-C_r ScR_e^2\overline{Q}(r,s) \quad (8)$$

On applying the corresponding condition $\overline{Q}(r,0)=0$ into equation (8) we obtain

$$ScR_e s^{\alpha}\overline{Q}(r,s)=\left[\frac{\partial^2\overline{Q}(r,s)}{\partial\bar{r}^2}+\frac{1}{\bar{r}}\frac{\partial\overline{Q}(r,s)}{\partial\bar{r}}\right]-C_r ScR_e^2\overline{Q}(r,s) \quad (9)$$

On rearranging (9) we obtain

$$\frac{\partial^2\overline{Q}(r,s)}{\partial\bar{r}^2}+\frac{1}{\bar{r}}\frac{\partial\overline{Q}(r,s)}{\partial\bar{r}}-\lambda_{\emptyset}^2\overline{Q}=0. \quad (10a)$$

Where

$$\lambda_{\emptyset}^2=ScR_e(s^{\alpha}+C_rR_e). \quad (10b)$$

Multiplying equation (10a) by r^2 gives

$$r^2 \frac{\partial^2 \overline{Q}(r,s)}{\partial \bar{r}^2} + r \frac{\partial \overline{Q}(r,s)}{\partial \bar{r}} - r^2 \lambda_{\emptyset}^2 \overline{Q} = 0. \quad (11)$$

Equation (11) is the modified Bessel equation of order zero, which have the general solution of

$$\overline{Q}(r,s) = C_1(s) Io(\lambda_{\emptyset} r) + C_2(s) K_0(\lambda_{\emptyset} r), \quad (12)$$

Where Io and K_0 are the modified Bessel functionof the $1^{st} and\ 2^{nd}$ kinds.

Applying the center line condition $r = 0$,the function $K_0(\lambda_{\emptyset} r)$ is singular at $r = 0$.

Therefore, to satisfy the condition

$$\left.\frac{\partial Q}{\partial r}\right|_{r=0} = 0\ , \quad \ldots (13)$$

and ensure boundedness at the centerline, we must set $C_2(s) = 0$.

Hence, equation (12) becomes.

$$\overline{Q}(r,s) = C_1(s) Io(\lambda_{\emptyset} r) \quad \ldots (14)$$

Apply the wall boundary condition $r = R(z)$

Using

$$\overline{Q}(R(z),s) = 0, \quad \ldots (15)$$

We obtain:

$$C_1(s) Io(\lambda_{\emptyset} r) = 0 \quad \ldots (16)$$

For non-trivial solution, $C_1(s) \neq 0$, this implies the eigen value condition:

$$Io(\lambda_{\emptyset} R(z)) = 0 \quad \ldots (17)$$

Let

β_n denote the positive roots of equation (51), such that:

$$\lambda_n = \frac{\beta_n}{R(z)}, \quad n = 1,2,3, \ldots \quad \ldots (18)$$

The solution of the concentration equation (44) can therefore be written as a series solution:

$$\overline{Q}(r,s) = \sum_{n=1}^{\infty} A_n(s) I_0\left(\frac{\beta_n r}{R(z)}\right) \quad \ldots (19)$$

Where $\boldsymbol{\beta_n}$ are the root of $I_0(\beta_n) = 0$

Using the definition of $\lambda_{\emptyset}^2$ (equation 45b) and standard inverse Laplace transform for Caputo fractional operators, the time domain becomes:

$$Q(r,t) = \sum_{n=1}^{\infty} A_n I_0\left(\frac{\beta_n r}{R(z)}\right) E_\alpha\left[-\left(C_r R_e + \frac{\beta_n^2}{ScR_eR^2(z)}\right)t^\alpha\right] \quad (20)$$

Where $E_\alpha(.)$ is the Mittag-Leffler function.

The coefficients A_n are determined from the orthogonality property of the modified Bassel function. They are obtaining by expanding the initial concentration distribution $Q(r,0)$ in terms of the eigen function $I_0\left(\frac{\beta_n r}{R(z)}\right)$, Using:

$$A_n = \frac{\int_0^{R(z)} rQ(r,0)I_0\left(\frac{\beta_n r}{R(z)}\right)dr}{\int_0^{R(z)} r\left[I_0\left(\frac{\beta_n r}{R(z)}\right)\right]^2 dr} \quad (21)$$

From the physical formular of the problem, the concentration is initially uniform across the arterial cross section hence,

$$Q(r,0) = 1 \quad (22)$$

Evaluating the numerator of equation (21) we have

$$\int_0^{R(z)} rI_0\left(\frac{\beta_n r}{R(z)}\right)dr \quad \ldots (23)$$

$$\text{Let } \xi = \frac{\beta_n r}{R(z)} \Rightarrow dr = \frac{R(z)}{\beta_n}d\xi \quad \ldots (24)$$

Then (23) gives:

$$\int_0^{R(z)} \frac{R^2(z)}{\beta_n^2}\xi I_0(\xi)d\xi \quad \ldots (25)$$

Using the standard identity

$$\int \xi I_0(\xi)d\xi = \xi I_1(\xi) \quad \ldots (26)$$

We obtain the numerator of (21) to be:

$$\frac{R^2(z)}{\beta_n^2}[\xi I_1(\xi)]_0^{\beta_n} = \frac{R^2(z)}{\beta_n} I_1(\beta_n) \quad \ldots (27)$$

Similarly for the denominator of (21) we have:

$$\int_0^{R(z)} r\left[I_0\left(\frac{\beta_n r}{R(z)}\right)\right]^2 dr = \frac{R^2(z)}{2}[I_0^2(\beta_n) + I_1^2(\beta_n)] \quad \ldots (28)$$

Note: we use the standard Bessel integral identity

On substituting (27) and (28) into (21) we have:

$$A_n = \frac{2I_1(\beta_n)}{\beta_n[I_0^2(\beta_n)+I_1^2(\beta_n)]} \quad \ldots (29)$$

Hence equation (54) becomes:

$$Q(r,t) = \sum_{n=1}^{\infty} \frac{2I_1(\beta_n)}{\beta_n[I_0^2(\beta_n)+I_1^2(\beta_n)]} I_0\left(\frac{\beta_n r}{R(z)}\right) E_\alpha\left[-\left(C_r R_e + \frac{\beta_n^2}{ScR_e R^2(z)}\right) t^\alpha\right] \quad \ldots (30)$$

Where:

$$I_0 = \sum_{k=0}^{\infty} \frac{1}{(k!)^2}\left(\frac{x}{2}\right)^{2k} \text{ and } I_1 = \sum_{k=0}^{\infty} \frac{1}{k!(k+1)!}\left(\frac{x}{2}\right)^{2k+1} \quad \ldots (31)$$

$$\text{Thus, } I_0\left(\frac{\beta_n r}{R(z)}\right) = \sum_{k=0}^{\infty} \frac{1}{(k!)^2}\left(\frac{\beta_n^2 r^2}{4R^2(z)}\right)^k \quad \ldots (32)$$

$$E_\alpha\left(-\lambda_\phi t^\alpha\right) = \sum_{m=0}^{\infty} \frac{\left(-\lambda_\phi t^\alpha\right)^m}{\Gamma(\alpha m+1)} \quad \ldots (33)$$

Where

$$\lambda_\phi = C_r R_e + \frac{\beta_n^2}{ScR_e R^2(z)} \quad \ldots (34)$$

Hence equation (30) becomes:

$$Q(r,t) = \sum_{n=1}^{\infty} \frac{2I_1(\beta_n)}{\beta_n[I_0^2(\beta_n)+I_1^2(\beta_n)]} \sum_{k=0}^{\infty} \cdot \sum_{m=0}^{\infty} \frac{(-1)^m}{(k!)^2\Gamma(\alpha m+1)} \left(\frac{\beta_n^2 r^2}{4R^2(z)}\right)^k \left[-\left(C_r R_e + \frac{\beta_n^2}{ScR_e R^2(z)}\right) t^\alpha\right]^m \quad (35)$$

In truncated (practical form), keeping the first terms $(k = 0; m = 0,1)$, the solution may be approximated as:

$$Q(r,t) \approx \sum_{n=1}^{\infty} \frac{2I_1(\beta_n)}{\beta_n[I_0^2(\beta_n)+I_1^2(\beta_n)]} \left[1 + \frac{\beta_n^2 r^2}{4R^2(z)} - \frac{\left(C_r R_e + \frac{\beta_n^2}{ScR_e R^2(z)}\right) t^\alpha}{\Gamma(\alpha+1)}\right] \quad \ldots (36)$$

Results and Discussion

This section presents a detailed analysis of the analytical and numerical outcomes obtained from the developed mathematical model for blood flow through a stenosed artery. Emphasis is placed on validating the present model by comparing its predictions with well-

established results available in the literature. Such comparisons are essential to demonstrate the accuracy, reliability, and consistency of the extended formulation, especially in the presence of additional physical effects incorporated in the current study. Furthermore, the influence of key governing parameters on the flow and transport characteristics is examined to highlight the physiological relevance of the results and the improvements achieved over previous models.

Table 1 presents a comparative analysis of the axial velocity profile of a Maxwell fluid as a function of the radial coordinate r, comparing the results of Kot and Elmabound (2021), Wang et al. (2022), and the present study. At the centerline of the artery (r=0), all three studies predict the same maximum velocity value, indicating perfect agreement and confirming the correctness of the imposed symmetry condition at the arterial core.

As the radial distance increases toward the arterial wall, a gradual decrease in velocity is observed across all models, which is consistent with the no-slip boundary condition at the wall. However, the present study consistently predicts slightly higher velocity values compared to the earlier works. This deviation becomes more noticeable near the arterial wall, suggesting that the additional physical effects incorporated in the current model such as porous medium resistance, magnetic field influence, and nanoparticle interactions enhance momentum transport within the blood flow. The close numerical agreement across all radial positions demonstrates that the present model not only aligns well with previous studies but also provides a refined and more comprehensive representation of the flow dynamics

Figure 2 illustrates the graphical validation of the axial velocity profile u(r,t) obtained in the present study against the results reported by Kot & Elmabound (2021) and Wang et al. (2022). The velocity distribution exhibits a smooth parabolic-like profile, with maximum velocity at the centerline and a monotonic decline toward the arterial wall, which is characteristic of laminar blood flow in stenosed arteries.

A strong overlap between the curves is observed, indicating excellent agreement between the three studies. The slight elevation of the present velocity profile across the radial domain further confirms the influence of the additional modeled parameters without altering the fundamental flow behavior. This close correspondence validates the analytical procedure adopted in the current work and confirms that the extended model preserves the physical integrity of classical results while offering improved descriptive capability for complex physiological conditions

Table 1; Comparative analysis of the Maxwell fluid velocity profile of previous studies with the current research work

Radius (r)	Kot & Elmabound (2021)	Wang et al. (2022)	Present Study
0.0	5.000000	5.000000	5.000000
0.1	4.982065	4.985045	4.986039
0.2	4.964129	4.970090	4.972078
0.3	4.911092	4.925760	4.930662
0.4	4.858054	4.881429	4.889245
0.5	4.772164	4.809295	4.821745
0.6	4.686274	4.737161	4.754245
0.7	4.571107	4.639741	4.662865
0.8	4.455939	4.542320	4.571484
0.9	4.316145	4.422930	4.459138
1.0	4.176351	4.303540	4.346791
0.1	4.982065	4.985045	4.986039

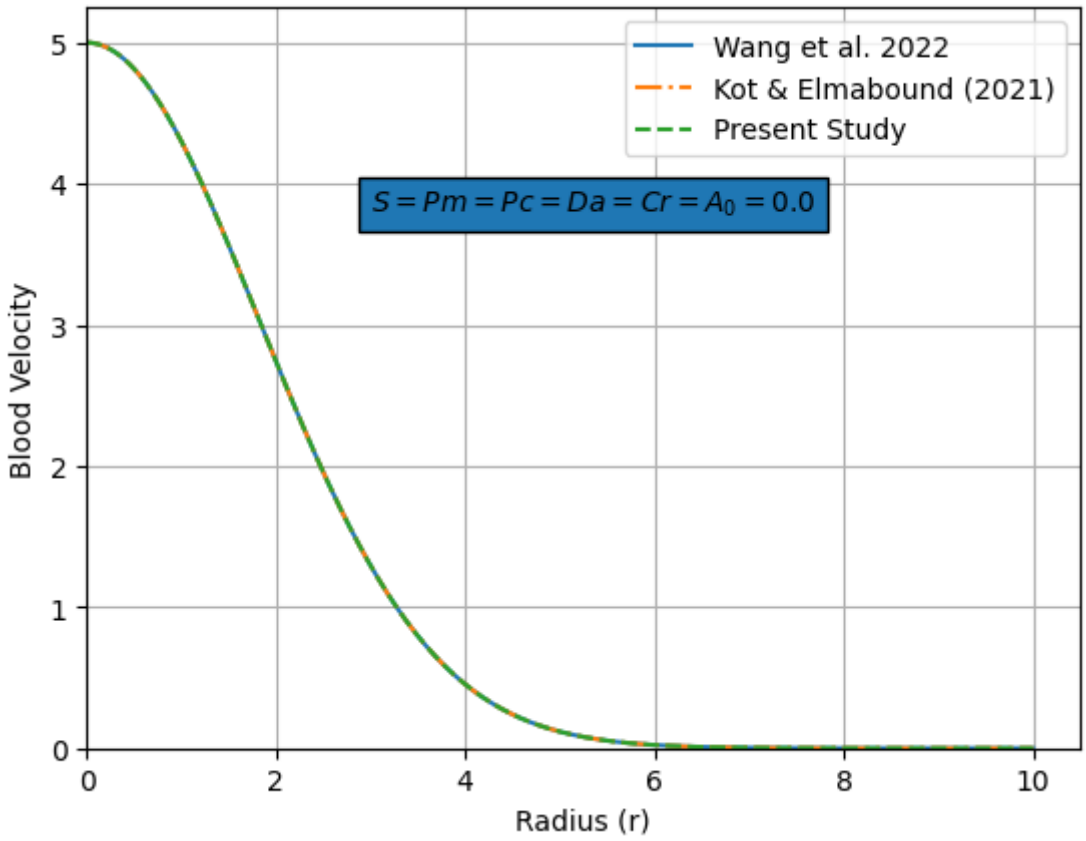

Figure 2. *The validation and comparison of the axial velocity u (r, t) profile of blood flow with the previous work of Wang et al., 2022.*

Analysis of the main results

This section presents the numerical solutions equations (34). The parameters used in this study were assigned the following values based on the literature:

$$Ha = 0.5, Cr = 0.5, Sc = 0.5, \alpha = 0.1, Ec = 0.5, Sr = 0.5, Ra = 0.5, \Pr = 20.0, \mathrm{Re} = 2.0, Br = 10.0$$
$$Da = 0.1, Gc = 0.5, Gr = 0.5, \omega = \pi/4, P_m = 0.5, P_C = 0.5, \lambda = 0.015, \lambda_1 = 0.1, Pe = 5.0,$$
$$S = Q_s = 0.5, A_0 = 2.0, k = 0.1, \Phi = 60^0$$

Figure 3 illustrates the influence of the chemical reaction parameter on the concentration distribution of nanoparticles (or solute species) within the stenosed arterial segment. It is observed that an increase in the chemical reaction parameter leads to a significant reduction in concentration levels across the radial direction of the artery. Physically, a higher chemical reaction parameter corresponds to an intensified reaction rate, which enhances the consumption or decay of nanoparticles within the blood flow. As a result, the species are depleted more rapidly, leading to lower concentration values throughout the arterial domain. The concentration remains maximum near the centerline and decreases toward the arterial wall, consistent with diffusion-dominated transport and boundary constraints. This behavior confirms that chemical reactions play a critical role in regulating mass transport in biological flows, particularly in drug delivery and nanoparticle-assisted therapies.

Figure 4 depicts the effect of the Schmidt number (Sc) on the concentration profile. The results show that increasing the Schmidt number causes a decrease in nanoparticle concentration throughout the flow field. The Schmidt number represents the ratio of momentum diffusivity to mass diffusivity. Higher Schmidt numbers imply lower mass diffusivity, which restricts the diffusion of nanoparticles within the blood flow. Consequently, species transport becomes weaker, resulting in thinner concentration boundary layers and reduced concentration values. This trend highlights the dominance of viscous effects over molecular diffusion at higher Schmidt numbers and is particularly relevant in physiological flows where blood viscosity significantly affects solute transport.

Figure 5 demonstrates the influence of the fractional-order parameter on the concentration distribution. It is evident that increasing the fractional order enhances the concentration level across the arterial radius. This behavior can be attributed to the memory effect inherent in fractional-order models. Lower fractional orders correspond to stronger

memory effects, which slow down diffusion and mass transport processes. As the fractional order increases, these memory effects weaken, allowing nanoparticles to diffuse more effectively within the blood flow. Consequently, higher fractional orders result in increased concentration levels and a smoother concentration distribution. This result confirms the suitability of fractional calculus in capturing anomalous diffusion and hereditary effects in biological transport phenomena.

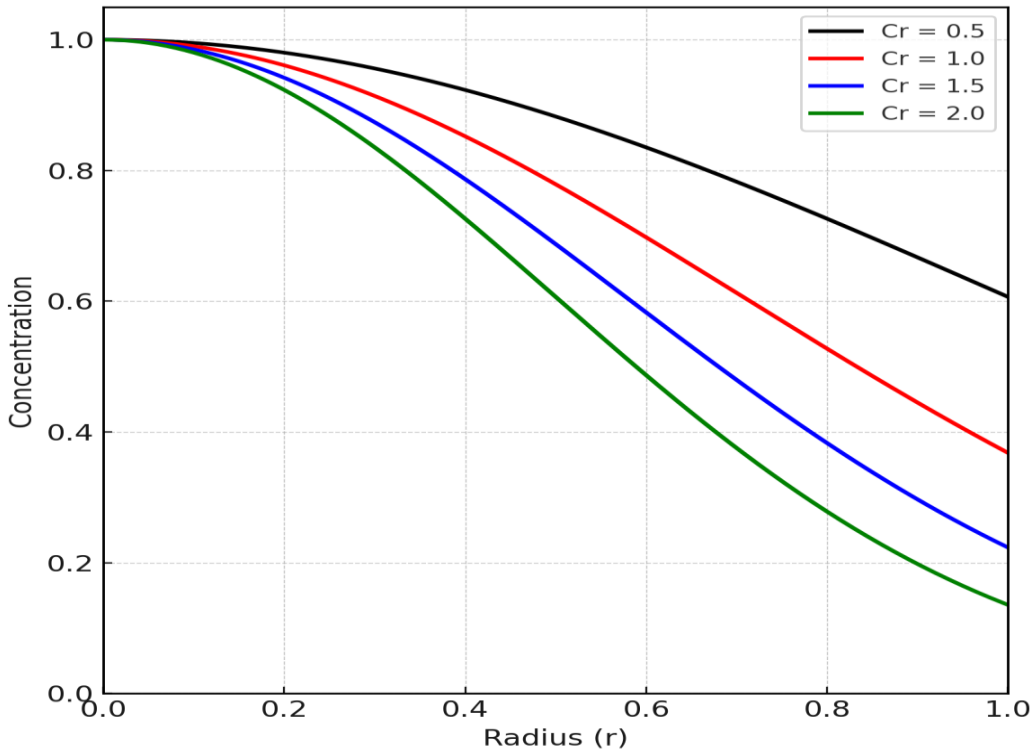

Figure 3: Effect of Chemical Reaction Parameter on the Concentration profile

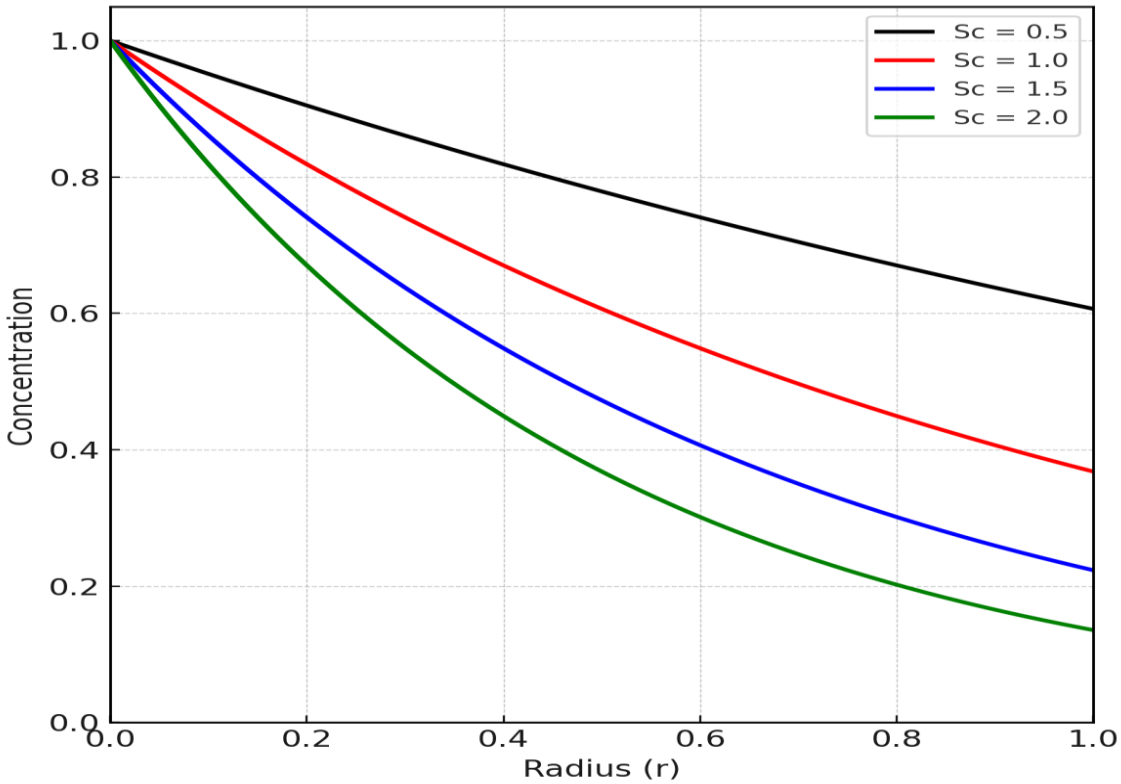

Figure 4: Effect of Schmidt number on the Concentration profile

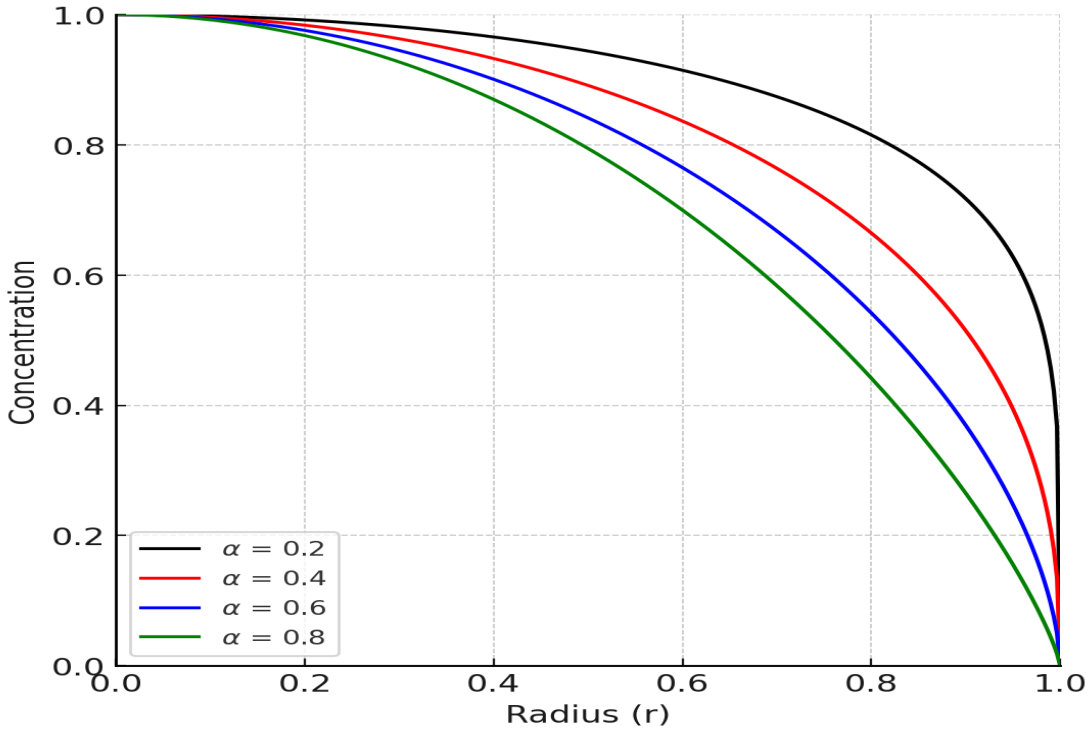

Figure 5: Effect of Fractional order on the Concentration profile

Conclusion

An extended fractional-order model for blood flow through a stenosed artery has been developed and analyzed by incorporating magnetic field effects, porous medium resistance, chemical reaction, and nanoparticle diffusion. Semi-analytical solutions were obtained and validated through close agreement with existing studies. The results show that chemical reaction and Schmidt number reduce nanoparticle concentration, while increasing the fractional order enhances mass transport by weakening memory effects. The study confirms that fractional calculus provides an effective framework for modeling complex transport phenomena in biological blood flow and improves the physical realism of stenosed artery models.

Recommendations

a) The present model can be extended to include more realistic non-Newtonian blood rheology to better capture physiological blood flow behavior in diseased arteries.

b) Future studies may incorporate spatial fractional derivatives and variable-order fractional models to further improve the description of anomalous diffusion and memory effects in biological transport processes.

c) The inclusion of arterial wall elasticity and fluid structure interaction is recommended to enhance the physiological relevance of the model.

d) Numerical simulations and experimental or clinical data should be employed to validate and calibrate the analytical results for practical biomedical applications.

e) The modeling framework may be applied to drug delivery and nanoparticle-based therapeutic systems to assess transport efficiency in stenosed arteries.

References

Adamu, H. A., Abubakar, M. B., & Danladi, A. M. (2020). MHD flow of blood through stenosed arteries under the influence of inclined magnetic field. *Scientific African, 8*, e00409.

Ahmed, S. A., & Giddens, D. P. (1983). Flow disturbance measurements through a constricted tube at moderate Reynolds numbers. *Journal of Biomechanics, 16*(12), 955–963. https://doi.org/10.1016/0021-9290(83)90096-9

Alhachami, A. S. K., Asadi, Z., Jalili, B., Khan, Y., ShayanMehr, M., Jalili, P., & Ganji, D. D. (2024). Hydrothermal analysis of time-fractional magneto hydrodynamic viscous fluid flow on a plate. *ZAMM – Zeitschrift für Angewandte Mathematik und Mechanik, 104*(11), e202300369. https://doi.org/10.1002/zamm.202300369

Buongiorno, J. (2006). Convective transport in nanofluids. *Journal of Heat Transfer, 128*(3), 240–250. https://doi.org/10.1115/1.2150834

Chamkha, A. J., & Ben-Nakhi, A. (2008). MHD mixed convection-radiation interaction along a permeable surface immersed in a porous medium in the presence of Soret and Dufour's effects. *Heat and Mass Transfer, 44*(7), 845–856. https://doi.org/10.1007/s00231-007-0296-x

Che, H., Wang, Y. L., & Li, Z. Y. (2022). Novel patterns in a class of fractional reaction–diffusion models with the Riesz fractional derivative. *Mathematics and Computers in Simulation, 202*, 149–163. https://doi.org/10.1016/j.matcom.2022.05.037

Ellahi, R., Zeeshan, A., Hussain, F., & Asadollahi, A. (2019). Peristaltic blood flow of couple stress fluid suspended with nanoparticles under the influence of chemical reaction and activation energy. *Symmetry, 11*(2), 276. https://doi.org/10.3390/sym11020276

Ghasemi, B., Aminossadati, S. M., & Raisi, A. (2011). Magnetic field effect on natural convection in a nanofluid-filled square enclosure. *International Journal of Thermal Sciences, 50*, 1748–1756. https://doi.org/10.1016/j.ijthermalsci.2011.04.010

Han, C., Wang, Y. L., & Li, Z. Y. (2022). A high-precision numerical approach to solving space fractional Gray–Scott model. *Applied Mathematics Letters, 125*, 107759. https://doi.org/10.1016/j.aml.2021.107759

Hayat, T., Khan, M. I., Farooq, M., Alsaedi, A., Waqas, M., & Yasmeen, T. (2016). Impact of Cattaneo-Christov heat flux model in flow of variable thermal conductivity fluid over a variable thicked surface. *International Journal of Heat and Mass Transfer, 99*, 702–710. https://doi.org/10.1016/j.ijheatmasstransfer.2016.04.016

Horváth, G., Horváth, I., Almousa, S. A.-D., & Telek, M. (2020). Numerical inverse Laplace transformation using concentrated matrix exponential distributions. *Performance Evaluation, 137*, 102067. https://doi.org/10.1016/j.peva.2019.102067

Hussain, S., Murtaza, M. G., & Nadeem, S. (2019). Influence of hybrid nanoparticles on the peristaltic flow of Carreau fluid in a non-uniform tube. *Computer Methods and Programs in Biomedicine, 177*, 141–152.

Imoro, I., Etwire, C. J., & Musah, R. (2024). MHD flow of blood-based hybrid nanofluid through a stenosed artery with thermal radiation effect. *Case Studies in Thermal Engineering, 59*, 104418. https://doi.org/10.1016/j.csite.2024.104418

Isah, A., Musa, A., Yakubu, G., Adamu, G. T., Mohammed, A., Baba, A., Kadas, S., & Mahmood, A. (2024). The impact of heat source and chemical reaction on MHD blood flow through permeable bifurcated arteries with tilted magnetic field in tumor treatments. *Computer Methods in Biomechanics and Biomedical Engineering, 27*(5), 558–569. https://doi.org/10.1080/10255842.2023.2190833

Jamil, D. F., Saleem, S., Roslan, R., Al-Mubaddel, F. S., Rahimi-Gorji, M., Issakhov, A., & Din, S. U. (2021). Analysis of non-Newtonian magnetic Casson blood flow in an inclined stenosed artery using Caputo-Fabrizio fractional derivatives. *Computer Methods and Programs in Biomedicine, 203*, 106044. https://doi.org/10.1016/j.cmpb.2021.106044

Jamil, M., Khan, M., Khan, W. A., & Ayaz, M. (2016). Unsteady MHD flow of viscoelastic fluid in a channel with heat and mass transfer. *AIP Advances, 6*(3), 035214.

Khanafer, K., Vafai, K., & Lightstone, M. (2003). Buoyancy-driven heat transfer enhancement in a two-dimensional enclosure utilizing nanofluids. *International Journal of Heat and Mass Transfer, 46*(19), 3639–3653. https://doi.org/10.1016/S0017-9310(03)00156-X

Khan, M., Shah, F., & Islam, S. (2015). Effects of chemical reaction on MHD mixed convection flow of nanofluid over a stretching sheet. *Journal of the Taiwan Institute of Chemical Engineers, 50*, 119–128.

Kot, P., & Elmabound, A. (2021). Analysis of pulsatile blood flow through a stenosed artery using fractional calculus. *Mathematics, 9*(3), 210.

Mahanthesh, B., Gireesha, B. J., & Gorla, R. S. R. (2017). Mixed convection flow of a dusty nanofluid over a stretching sheet embedded in a porous medium with thermal radiation and heat source/sink effects. *Journal of Nanofluids, 6*(4), 702–710.

Nazar, T., & Shabbir, M. S. (2023). Irreversibility analysis in the ternary nanofluid flow through an inclined artery via Caputo-Fabrizio fractional derivatives. *Results in Physics, 53*, 106992. https://doi.org/10.1016/j.rinp.2023.106992

Sandeep, N., & Kumar, B. R. (2016). Effects of inclined magnetic field on flow of a nanofluid over a stretching surface with chemical reaction and radiation. *Journal of Molecular Liquids, 221*, 108–115.

Sheikholeslami, M. (2018). Influence of Lorentz forces on nanofluid flow in a porous cylinder considering Brownian motion. *Journal of Molecular Liquids, 258*, 518–526.

Sheikholeslami, M., & Ganji, D. D. (2016). Ferrohydrodynamic and magnetohydrodynamic effects on ferrofluid flow in a permeable channel with aligned magnetic field. *Journal of Molecular Liquids, 217*, 490–497.

Sheikholeslami, M., Gorji-Bandpy, M., Ganji, D. D., Soleimani, S., & Seyyedi, S. M. (2015). Natural convection of nanofluids in a cavity with thick bottom wall in the presence of magnetic field. *International Journal of Heat and Mass Transfer, 80*, 16–25.

Sheikholeslami, M., & Rokni, H. B. (2017). Nanofluid heat transfer in a permeable cavity considering Brownian motion and thermophoresis effects. *Journal of Molecular Liquids, 233*, 288–296.

Shit, G. C., & Majee, S. (2015). Pulsatile flow of blood and heat transfer with variable viscosity under magnetic and vibration environment. *Journal of Magnetism and Magnetic Materials, 388*, 106–115. https://doi.org/10.1016/j.jmmm.2015.04.026

Tripathi, D., Bég, O. A., & Javed, M. Y. (2018). Unsteady flow of viscoelastic nanofluids in a flexible tube with heat and mass transfer. *Journal of Mechanics in Medicine and Biology, 18*(3), 1850024.

Wang, X., Qiao, Y., Qi, H., & Xu, H. (2022). Numerical study of pulsatile non-Newtonian blood flow and heat transfer in small vessels under a magnetic field. *International Communications in Heat and Mass Transfer, 133*, 105930. https://doi.org/10.1016/j.icheatmasstransfer.2022.105930

Yakubu, D. G., Abdullahi, I., & Musa, A. (2025). The dynamic flow of ternary nanofluids with magnetic nanoparticles in an inclined artery exposed to thermal radiation and magnetic fields. *Alexandria Engineering Journal, 123*, 231–241. https://doi.org/10.1016/j.aej.2025.01.056